Approximating k_{zc}, k_{xc}, and ξ_c by k_z, k_x, and ξ, respectively, coupling factor K_x is given by the following equations:

$$K_x = \sin\left(2\int_0^{\frac{\pi}{2}} \frac{k_{zsc}-k_{zac}}{2}\,d\theta\right) \tag{B-6}$$

$$= \sin\left\{4\frac{k_x^2\xi R}{k_z a(1+k_x^2\xi^2)}\int_0^{\frac{\pi}{2}} \cdot\exp\left[-\frac{\theta\{d_x+2(R+a/2)(1-\cos\theta)\}}{\xi\sin\theta}\right]d\theta\right\}. \tag{B-7}$$

ACKNOWLEDGMENT

The authors wish to thank M. Shinji and I. Ohtomo, of the Yokosuka Electrical Communication Laboratory, for their invaluable advice.

REFERENCES

[1] E. A. J. Marcatili, "Dielectric rectangular waveguide and directional coupler for integrated optics," *Bell Syst. Tech. J.*, vol. 48, pp. 2071–2102, Sept. 1969.
[2] J. E. Goell, "A circular-harmonic computer analysis of rectangular dielectric waveguides," *Bell Syst. Tech. J.*, vol. 48, pp. 2133–2160, Sept. 1969.
[3] R. M. Knox and P. P. Toulios, "Integrated circuits for the millimeter–optical-frequency range," *Proc. Symp. Submillimeter Waves*, New York, NY, Mar. 1970.
[4] E. A. J. Marcatili and S. E. Miller, "Improved relations describing directional control in electromagnetic wave guidance," *Bell. Syst. Tech. J.*, vol. 48, pp. 2161–2188, Sept. 1969.
[5] E. A. J. Marcatili, "Bends in optical dielectric guides," *Bell Syst. Tech. J.*, vol. 48, pp. 2103–2132, Sept. 1969.
[6] I. Ohtomo, "Channel dropping filters using ring resonators for a millimeter-wave communication system," in *Rev. Elec. Commun. Lab.*, N.T.T. Pub. Corp., Japan, vol. 19, nos. 1–2, pp. 87–98. Jan.–Feb. 1971.
[7] E. G. Neumann and H. D. Rudolph, "Radiation from bends in dielectric rod transmission lines," *IEEE Trans. Microwave Theory Tech.*, vol. MTT-23, pp. 142–149, Jan. 1975

Silicon Waveguide Frequency Scanning Linear Array Antenna

KENNETH L. KLOHN, MEMBER, IEEE, ROBERT E. HORN, MEMBER, IEEE, HAROLD JACOBS, FELLOW, IEEE, AND ELMER FREIBERGS, MEMBER, IEEE

***Abstract*—The design and experimental findings of a novel approach for a relatively simple low-cost frequency-scanning millimeter-wave antenna are described. The antenna consists of a silicon dielectric rectangular rod with periodic metallic stripe perturbations on one side. The feasibility of electronically scanning through a range of angles by varying the frequency fed into the silicon rod is shown. Calculations were made to determine the allowable physical size of the silicon rod in order to maintain a single fundamental mode of operation and the effect which size variations and perturbation spacing have on the angle of radiation and the range of angular scan for a given frequency shift. Efforts covered the frequency range 55–100 GHz with specific points of interest at 60, 70, and 94 GHz. The results of the experiments conducted are compared with the theoretical calculations.**

I. INTRODUCTION

RECENT demands for a very high resolution radar in terminal homing for missiles and shells and for radar surveillance in general have generated a need for developing new concepts in low-cost millimeter-wave antennas. A means of providing electronic line scanning rather than mechanical scanning is desirable in order to reduce system complexity and high cost. It is especially important to eliminate the use of gimbals to mechanically scan an antenna since they are expensive and slow. This paper describes the design and experimental findings of a novel approach for a side-looking electronic line scanner consisting of a dielectric (silicon) rectangular rod with periodic perturbations on one side. Angular scan is achieved by varying the frequency, while the actual numerical values of the scan angles are a function of operating frequency, waveguide size (height and width), and perturbation spacing. Present work was concentrated in the range of 55–100 GHz.

The effect of varying the physical parameters will be shown, and comparisons will be made between theoretical calculations and experimental findings.

Manuscript received October 17, 1977; revised January 2, 1978. This work was supported by the U.S. Army In-House Laboratory Independent Research Program, Fort Monmouth, NJ.

The authors are with the U.S. Army Electronics Research and Development Command, Fort Monmouth, NJ 07703.

II. DESIGN CRITERIA

The key elements in the antenna design are operating frequency (in terms of λ_0), guide wavelength, and per-

turbation spacing. These three values determine the nth grating lobe angle of radiation as seen in the following equation [1], [2]:

$$\theta_n = \sin^{-1}\left(\frac{\lambda_0}{\lambda_g} + \frac{\lambda_0}{d}n\right), \qquad \left|\frac{\lambda_0}{\lambda_g} + \frac{\lambda_0}{d}n\right| \leq 1 \qquad (1)$$

where θ_n is the nth beam angle from broadside (normal), λ_0 is the free space wavelength, λ_g is the guide wavelength, d is the perturbation spacing, and n is the space harmonic $0, \pm 1, \pm 2, \cdots$.

The operating frequency in a system is chosen principally by application requirements such as resolution, range, and size of components. In a more practical sense, it depends on the availability of millimeter-wave power sources which are small, rugged, and reliable with sufficient power output for the intended application. The primary solid-state sources used to date have been Gunn and IMPATT diodes. Some preliminary work has been accomplished in incorporating these devices directly in dielectric waveguides at microwave frequencies where the guides are physically much larger than those studied in this paper [3]–[5]. The bulk of the experimental work reported here was done near 60 GHz where sufficient test equipment and power sources were available. Some work was completed at 70 GHz, and future experimental plans are aimed at 94 GHz.

The guide wavelength, for a given material and frequency, is determined by the physical size of the guide, i.e., width a and height b. Since it is advantageous from a practical point of view to avoid as much multisignal complexity as possible, single-mode operation must be maintained in the propagation of energy in the waveguide with only a single beam of energy radiating from the antenna. Thus the designs presented in this paper which give the range (minimum and maximum) of guide sizes, allow only the E^y_{11} mode in the guide and the $n = -1$ space harmonic in the radiated energy.

Ideally, the waveguide should be kept as large as possible for any given frequency of operation as it eases fabrication problems and lessens the effect of size variations on the guide wavelength and scan angle. The maximum guide size is defined as that above which multiple-mode operation is possible. The minimum guide size is defined as that below which the electric field becomes unguided. The maximum and minimum guide sizes were determined by calculating the propagation constants k_1, k_x, and k_y, as shown in Appendix A, using the transcendental equations formulated by Marcatili [6] and solving them exactly on a programmed calculator [7] using the relationship

$$k_z = \sqrt{k_1^2 - (k_x^2 + k_y^2)} \qquad (2)$$

which indicates that there is no propagation down the guide (z direction) when $(k_x^2 + k_y^2)$ exceeds k_1^2. Although Marcatili's approximate formula does not match precisely Goell's rigorous solution to the boundary value problem

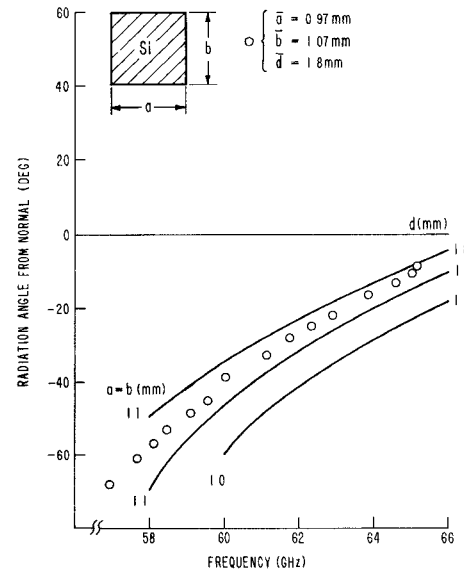

Fig. 1. Minimum and maximum waveguide dimensions: 60 GHz.

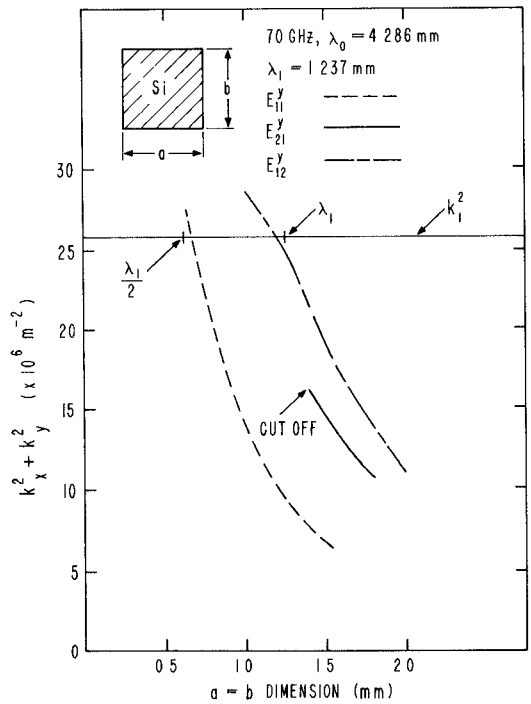

Fig. 2. Minimum and maximum waveguide dimensions: 70 GHz.

[8] and predict the fact that the fundamental E^y_{11} mode remains guided no matter how small the guide's cross section, we have found experimentally that (2) does give a good practical prediction for cutoff [9]. Figs. 1–3 were plotted for the fundamental E^y_{11} mode and the next two higher order modes E^y_{21} and E^y_{12} for the operating frequencies 60, 70, and 94 GHz. These plots show that the E^y_{12} mode is the limiting mode for maximum guide size if a unity aspect ratio ($a = b$) is to be maintained. However,

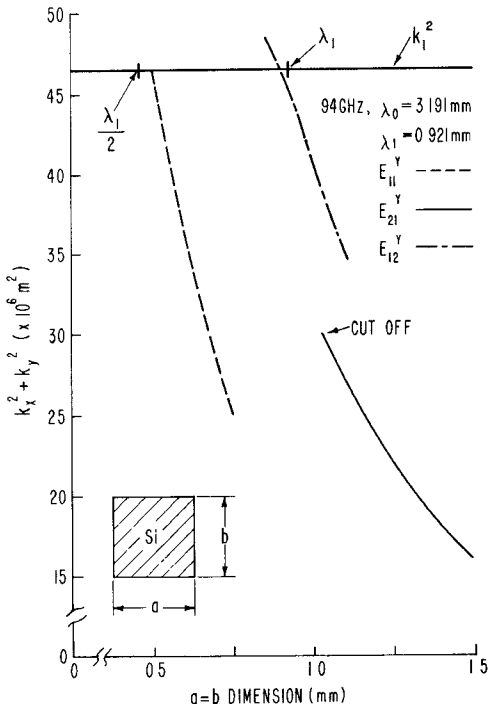

Fig. 3. Minimum and maximum waveguide dimensions: 94 GHz.

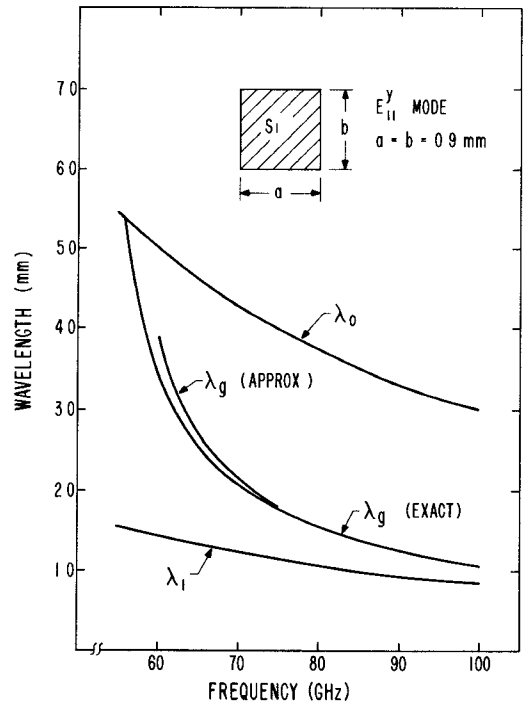

Fig. 4. Variation of wavelength with frequency.

TABLE I
MINIMUM AND MAXIMUM WAVEGUIDE SIZES FOR FUNDAMENTAL MODE E_{11}^y

FREQUENCY (GHz)	GUIDE SIZE (mm) MIN	$\lambda_1/2$	MAX	λ_1
60	0.775	0.772	1.4	1.443
70	0.67	0.619	1.2	1.237
94	0.50	0.416	0.9	0.921

TABLE II
COMPARISON OF EXACT AND APPROXIMATE VALUES FOR GUIDE WAVELENGTH

FREQUENCY(GHz)	EXACT(mm)	APPROX(mm)	$\Delta\lambda_g$(mm)	% DIFFERENCE
60	3.431	3.900	0.469	13.7
70	2.069	2.125	0.056	2 7
80	1.552	1.568	0.016	1 0
90	1.262	1.269	0.007	0.6

since k_x is independent of the guide height, the guide width could be made somewhat larger than the guide height: the limiting value being the cutoff point (size below which the mode will not propagate) for the E_{21}^y mode. The figures also indicate that λ_1, the wavelength in an infinite medium 1 (silicon in this case), can be used as a good first-order approximation for the maximum allowed guide size and $\lambda_1/2$ as the minimum guide size. The equation for λ_1 is

$$\lambda_1 = 2\pi n_1/\lambda_0 \tag{3}$$

where n_1 = index of refraction of medium 1. The figures for maximum and minimum guide size are listed in Table I. It is emphasized that these values are approximate. They do provide, however, a useful practical range of guide sizes to maintain single-mode operation at the indicated millimeter-wave frequencies. Later in this paper, experimental data will be correlated with theoretical calculations for silicon waveguides well within the boundaries of the predicted minimum and maximum sizes.

For any given waveguide size, the guide wavelength is also a function of operating frequency. Fig. 4 shows how the guide wavelength varies with frequency for a silicon guide, $a=b=0.9$ mm (maximum guide size for single-mode operation at 94 GHz). As the operating frequency falls below the design frequency, λ_g increases rapidly. The λ_g (approximate) curve shown in the figure was obtained by using the following simplifying assumptions (see Appendix A):

$$(k_x A_{3,5}/\pi)^2 \ll 1 \quad \text{and} \quad (k_y A_{2,4}/\pi)^2 \ll 1 \tag{4}$$

and then solving the transcendental equations in closed form. Table II shows the difference between λ_g (exact) and λ_g (approximate).

Above 80 GHz, $\Delta\lambda_g$ becomes relatively insignificant. The variation in guide wavelength when a and b are changed but kept equal to each other is shown in Fig. 5. The smaller the guide size, the larger λ_g will be; a 10-percent change in guide dimensions changes λ_g approximately 5 percent. It will be shown later in this paper how the changes in λ_g indicated in Figs. 4 and 5 affect the angle of radiation from periodic radiating elements. Once the physical dimensions of the dielectric guide are chosen for a given frequency, (in Fig. 1 $a=b=1.4$ mm is the maximum guide size for 60 GHz), the guide wavelength will be fixed for this frequency.

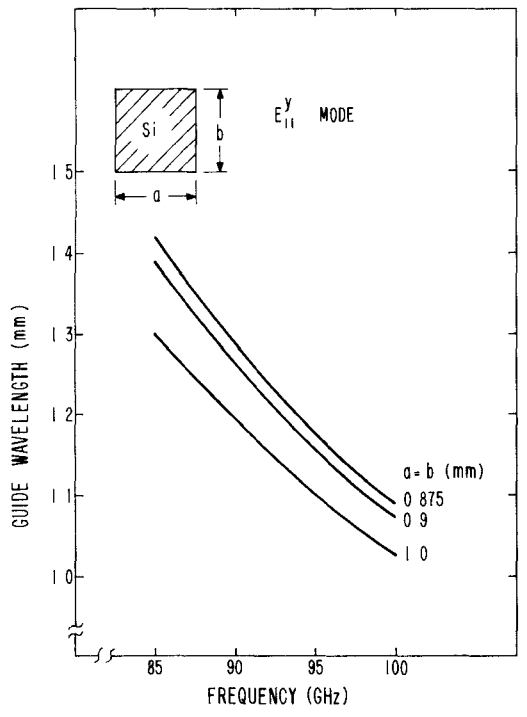

Fig. 5. Variation of guide wavelength with frequency as a function of size.

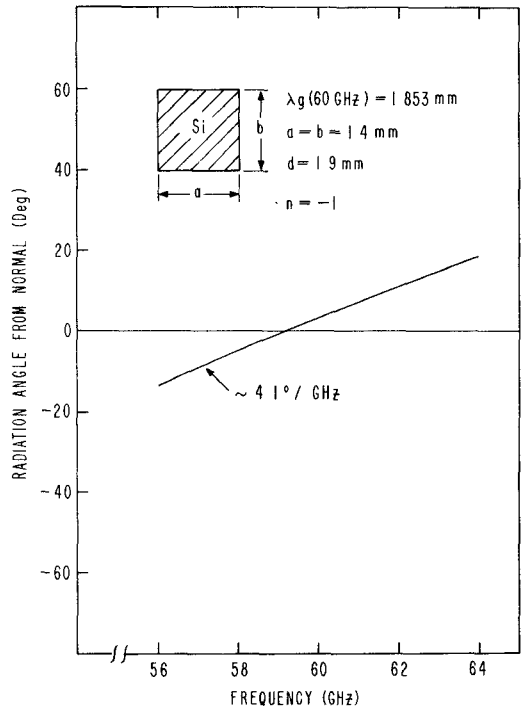

Fig. 6. Radiation angle versus frequency (60 GHz, design frequency).

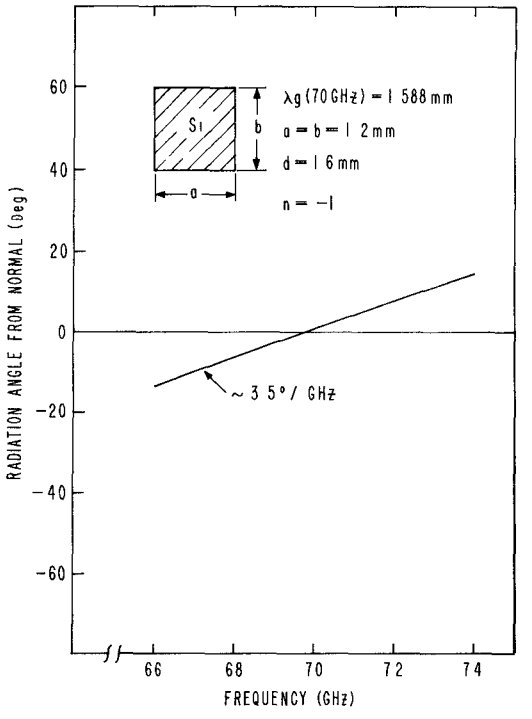

Fig. 7. Radiation angle versus frequency (70 GHz, design frequency).

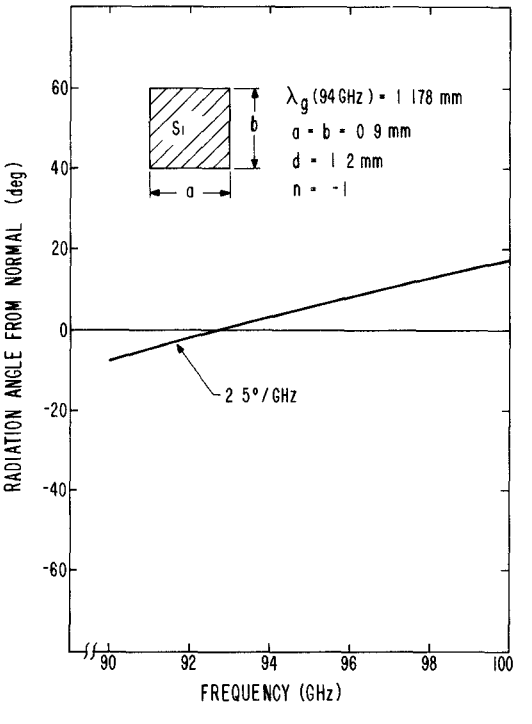

Fig. 8. Radiation angle versus frequency (94 GHz, design frequency).

Referring back to (1), we see that for a given space harmonic ($n=-1$ in our case) the only remaining variable to choose is the perturbation spacing d. To obtain broadside radiation at a given frequency, d must be chosen equal to the guide wavelength at that frequency thereby reducing θ_n to zero degrees. In actual practice, it is nearly impossible to match $d=\lambda_g$ exactly; therefore, the frequency at which $\theta_n=0°$ will be slightly different than the frequency designed to be zero.

III. Line Scan Angle

Figs. 6–8 give the angular scan theoretically possible (calculated from (1)) by varying the operating frequency $f_0 \pm 4$ GHz from the design frequency. A new set of propagation constants had to be calculated for each design frequency in order to determine the corresponding guide wavelength. It should be noted that the degrees of angular scan per GHz of frequency change decrease as

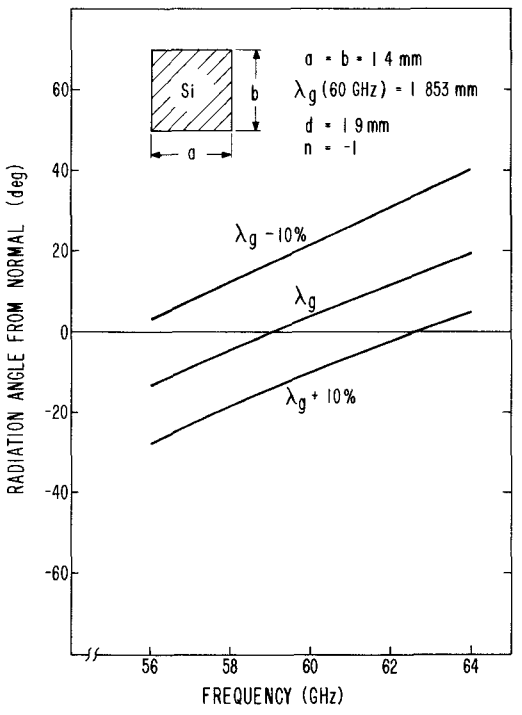

Fig. 9. Effect of λ_g on radiation angle.

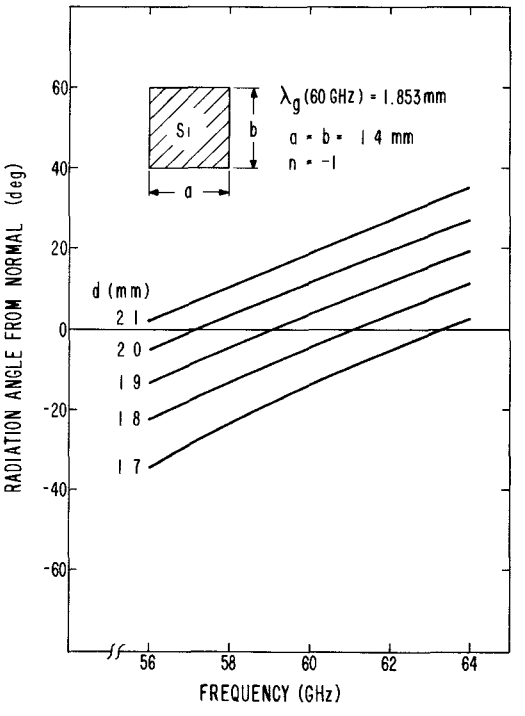

Fig. 10. Effect of perturbation spacing d on radiation angle.

the design frequency increases, i.e., 4.1°/GHz at 60 GHz, 3.5°/GHz at 70 GHz, and 2.5°/GHz at 94 GHz. In addition, for frequencies above the design frequency there is the possibility of higher modes propagating in the guide. Calculations indicate that radiation angles are very sensitive to changes or errors in λ_g. Experiments conducted to measure λ_g as a function of frequency indicated that the measured values always exceeded the calculated values [10]. Fig. 9 shows the effect on the radiation angle if λ_g is either ± 10 percent from the calculated value while the perturbation spacing is kept approximately equal to the calculated λ_g value. Over the frequency range examined, the scan angles for $\lambda_g - 10$ percent averaged $\sim 18°$ higher and for $\lambda_g + 10$ percent $\sim 14°$ lower than the angles calculated for λ_g.

As mentioned earlier, if the perturbation spacing is made equal to λ_g, the radiation will be normal to the waveguide at the design frequency. The entire range of angular scan, however, can be shifted more positively or negatively by changing the spacing of the perturbations, as shown in Fig. 10. Closer spacing shifts the angle more negatively, and, conversely, farther spacing shifts the angle more positively. The slope Δ degrees/Δ frequency remains essentially constant. For each 0.1-mm change in d, the radiation angle changes approximately 8°.

The range of scan angle, i.e., slope of the radiation angle curves, may be deliberately altered by changing the waveguide dimensions. As long as the dimensions stay between the minimum and maximum values, the energy will be guided, and no higher modes will appear. This is illustrated in Fig. 11. Smaller guide dimensions increase the slope thereby increasing the scan range for a given Δf_0. In each case, the perturbation spacing was adjusted

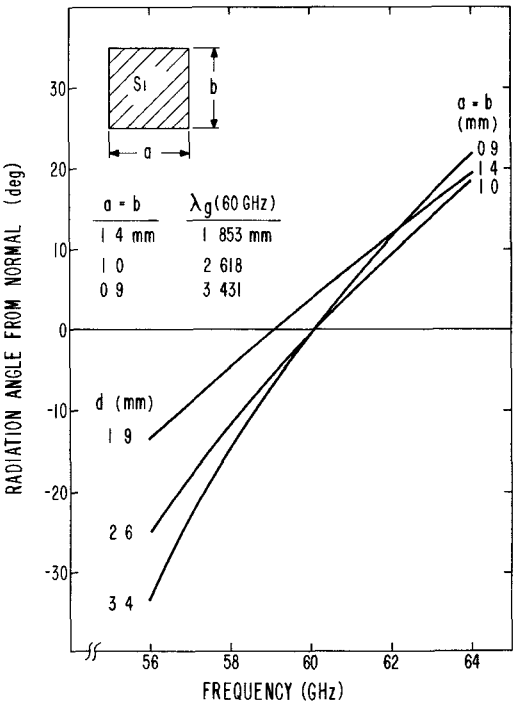

Fig. 11. Effect of guide size on angular scan with $d \approx \lambda_g$.

to match λ_g as closely as practical. The curve for $a = b = 1.4$ mm crosses $\theta = 0°$ at 59 GHz rather than 60 GHz because the perturbation spacing does not match λ_g as well as for $a = b = 0.9$ mm and $a = b = 1.0$ mm. The results are tabulated in Table III.

A variation of guide size and/or perturbation spacing could be used to adjust the scan range. Precautions would have to be taken to avoid multimoding which would add

TABLE III
ANGULAR SCAN FOR VARIOUS SIZE GUIDES ($\Delta f_0 = 8$ GHz)

GUIDE SIZE a=b	PERTURBATION SPACING, d	RANGE OF ANGULAR SCAN
0 9 mm	3.4 mm	56°
1.0	2.6	43°
1.4	1.9	33°

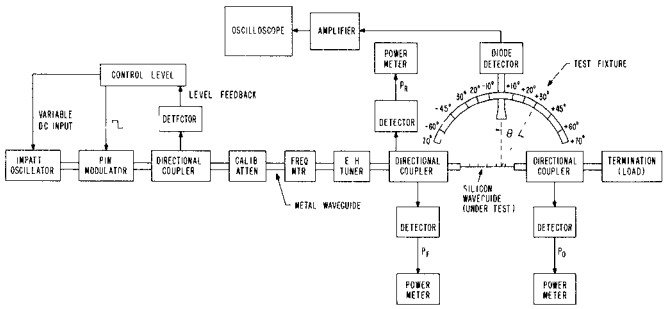

Fig. 12. Test setup for measurement of radiation angle θ versus frequency.

to the complexity of the system by producing more than one radiating beam.

IV. Experimental Results

The objectives of the following experiments were to determine if a silicon waveguide with surface perturbations is an effective radiating structure, if the radiated beam was less than 6° in the y–z plane where z is the direction down the guide and y is the vertical direction perpendicular to z, and if the beam is steerable as a function of frequency.

Numerous silicon waveguides were fabricated with various cross-sectional dimensions and lengths to determine their effect on the radiation angle and range of angular scan. The silicon waveguides, as covered in this paper, have dimensions of 0.969 mm×1.071 mm×10 cm for silicon waveguide B and 0.92 mm×0.91 mm×7 cm for silicon waveguide A.

A series of perturbations (grating structures) on the silicon waveguide are required to provide a radiating surface. A grating structure with grooves in a dielectric strip for use in a leaky wave antenna has been reported by Itoh [11]. The radiating structures covered in the following discussion used metal perturbations on the top of a rectangular silicon rod. The perturbations consisted of 16–22 rectangular copper foil stripes with dimensions of 0.3 mm×1 mm. The stripes were cemented to the top of the silicon to provide the perturbation structure. The distance from leading edge to leading edge of each metal stripe was set to an experimentally measured silicon waveguide wavelength λ_g as measured on an unperturbed silicon waveguide and checked with calculations using the Marcatili equations. The guide wavelength was measured using a test setup as shown in Fig. 12 without perturbing stripes on the silicon waveguide and without the radiation angle test fixture. A flanged metal waveguide horn

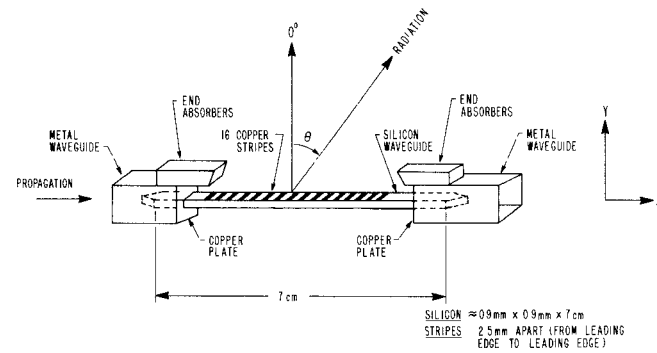

Fig. 13. Silicon waveguide with perturbations.

(terminated in a diode detector) was placed at a distance of less than 1 mm above the upper silicon surface in the near field of the propagated wave. The standing wave pattern on the silicon, produced by reflections due to an imperfect load, was then detected. The position between maxima points was measured using a calibrated micrometer. To obtain the average distance between maxima points, a large number of V_{max} measurements were made along the surface down the length of the guide.

The perturbation copper stripe spacing d was set equal to the measured λ_g. The perturbations covered a length of 4 cm using 16 stripes on the silicon waveguide. The silicon waveguide was then coupled to two adjoining metal waveguide sections using the thin copper foil end plates with 1-mm×1-mm center openings as shown in Fig. 13. The copper end plates provided the center support for coupling the metal wavegide to the silicon waveguide by positioning the silicon in the center of the metal waveguide. The pointed silicon waveguide extended about 1 cm into each of the two matching metal waveguide sections. In addition, the copper end plates provided a shield to prevent radiation from the metal waveguide into the air surrounding the silicon guide.

With the silicon waveguide mounted in the test holder as shown in Fig. 13, the test setup (Fig. 12) was assembled, and the radiation pattern from the silicon waveguide measured. The test setup was used to monitor forward power (P_f), reflected power (P_r), transmitted power (P_t), frequency (f_0), relative radiated power (P_{rad}) and radiation angle (θ). The flanged pickup horn (terminated in a diode detector and sensitive amplifier) was positioned at a distance of 20 cm from the exact center of the perturbation stripes. Most measurements were made at a 20-cm distance for mechanical convenience. However, measurements were also made at various distances in the far field (i.e., distances greater than 64 cm). The radiation patterns observed in the far field were almost identical with those observed at 20 cm. The flanged horn could then be positioned at any angle θ from $-85°$ to $+85°$ in the y–z plane on a calibrated test fixture. End absorbers (carbon compound material) were positioned directly over each end at the dielectric-to-metal waveguide transitions (Fig. 13) to prevent radiation leakage. The test setup used an IMPATT diode oscillator variable in frequency from 55 to

TABLE IV
PHYSICAL CHARACTERISTICS OF EXPERIMENTAL WAVEGUIDES

Silicon Waveguide	$\bar{a}$ width (Ave)	$\bar{b}$ height (Ave)	l length (overall)	n Number of Stripes	l_1 Length of Exposed Silicon	$\bar{d}$ Spacing between perturbation
A	0.91mm	0.92mm	7cm	16	5.4cm	0.25cm
B	0.969mm	1.071mm	10cm	22	8cm	0.18cm

63 GHz and a p-i-n diode modulator with a positive square wave modulation of about 1 kHz applied from the source. The p-i-n diode provided an amplitude modulated output down the waveguide and radiated out of the silicon surface. To prevent reflections from the metal waveguide to dielectric interface and thereby to keep the reflected power ratio P_r/P_{in} low, the silicon waveguide was matched to the metal guide by tapering both ends. It was found by experiment that the antenna VSWR was in the order of 1.4 over a wide range of frequencies and angles of radiation. However, as the angle of radiation approached 0°, the VSWR increased to about 3.0. This rise was gradual and started to appear at about 8° from normal. The transmitted power ratio (P_t/P_{in}) through the dielectric was in the range of 10 percent with a slight drop in the vicinity of 0°. This behavior is to be expected from theoretical considerations when λ_g approaches the perturbation spacing d.

The fraction of power radiated for a VSWR of 1.4 can be estimated by subtracting the fraction of power reflected ($P_r/P_{in} \sim 3$ percent) and power transmitted ($P_t/P_{in} \sim 10$ percent). The remaining 87 percent of the power is either radiated or lost as dissipation in the silicon or metal stripes. The dissipation losses in silicon measured in a millimeter-wave bridge were so small as to be negligible because of the high resistivity (30000 Ω·cm) of the material. We conclude that most of the power (87 percent) was radiated into free space.

Two experimental waveguides were prepared as indicated in Table IV. The radiation pattern of silicon waveguide B at a test frequency of 58.49 GHz is shown in Fig. 14(a). The polar plot of relative detected power shows a negative angle $\theta = -54°$ at the peak radiation point. The half-power points occur at 50 units which indicates a beamwidth of about 4°. The theoretical value for an aperture of 4 cm is 6°. The plot was obtained by arbitrarily setting the maximum value of radiated power at 100 units on the ac amplifier meter and moving the pickup horn through an angle $\pm\theta$ on either side of the peak to obtain the detected power plot as shown.

Fig. 14(b) shows a typical cross-sectional radiation pattern in the plane r–ϕ which is perpendicular to the plane shown in Fig. 14(a). Thus the three-dimensional radiation pattern is narrow in the y–z plane and wide in the r–ϕ plane. Point-by-point frequency tests on silicon waveguide B yielded the relationship between radiation angle θ and frequency as shown in Fig. 15. For frequencies between 57 and 65 GHz, the center of the radiated beam (θ_{max}) varied from −68 to −7°, a change of 7.5°/GHz. The above measurements were based on operation in the fundamental waveguide mode E_{11}^y. The 1-mm × 1-mm guide dimensions do not allow higher modes to propagate. The fact that these radiated beam angles are negative agrees with the theory. Since the dimensions of waveguide B are smaller than the calculated maximum for

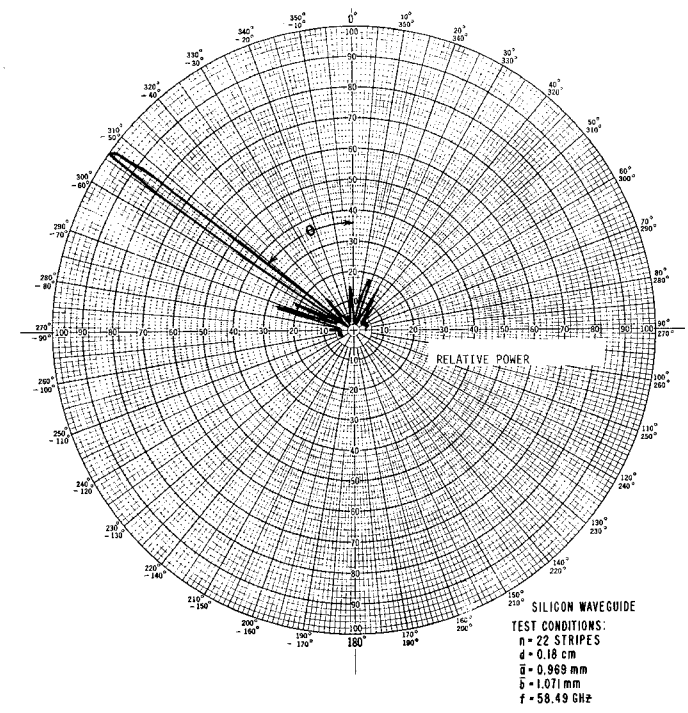

(a)

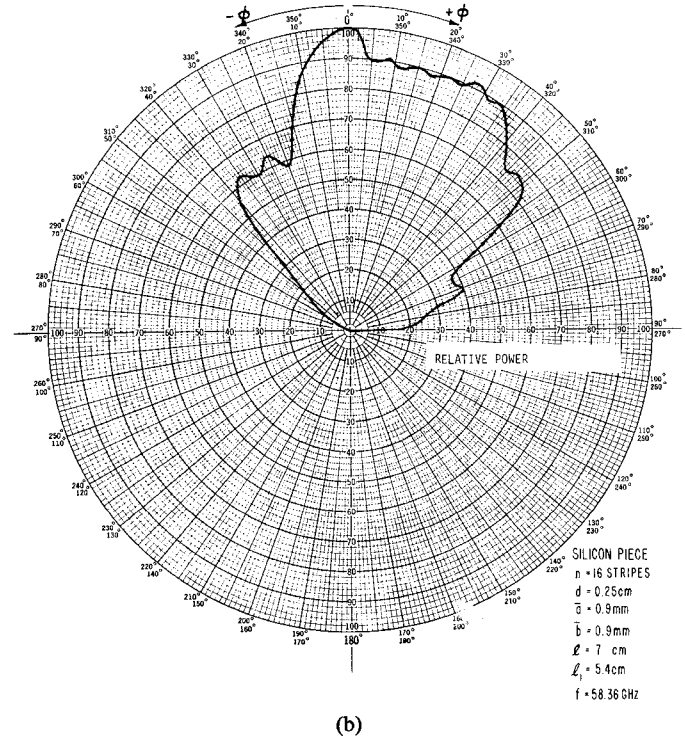

(b)

Fig. 14. Polar plot of beam angle. (a) y–z plane. (b) r–ϕ plane.

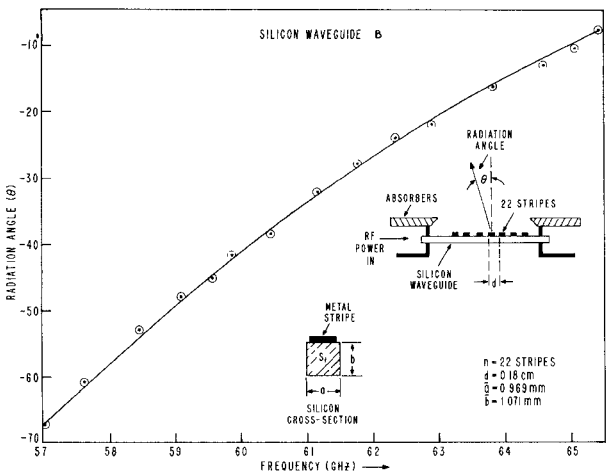

Fig. 15. Experimental plot of radiation angle versus frequency.

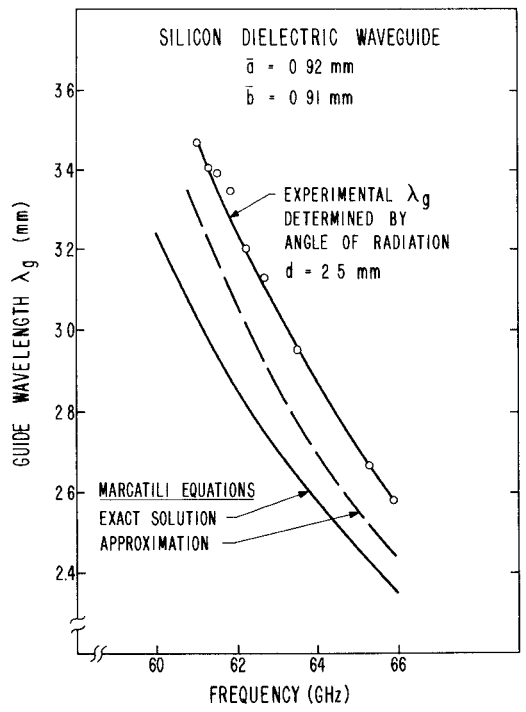

Fig. 16. Comparison of λ_g obtained experimentally from the radiation angle with theory.

~60-GHz operation, λ_g is larger than the 1.85-mm value predicted for the maximum guide size. Whenever the perturbation spacing is smaller than λ_g (1.8 mm was used for waveguide *B*) the effect is to shift the radiation angle more negatively as indicated in Fig. 10.

Using (1), λ_g can be estimated by measuring θ the angle of radiation and d the perturbation spacing. In Fig. 16 a plot was made of the guide wavelength λ_g for silicon waveguide *A* for dimensions 0.92 mm×0.91 mm with $d=2.5$ mm. The experimental λ_g is plotted from 61 to 66 GHz and is greater than the theoretical values (exact and approximate) obtained from the Marcatili equations.

The radiation angle θ (experimental and theoretical) versus the frequency for silicon waveguide *A* is plotted in Fig. 17(a). A comparison of the experimental and theoretical angles for $d=2.5$ mm indicates that the experimental values (circled points) are at a more negative angle than the theoretical values for $a=b=0.9$ mm but parallel as measured from frequencies of 62–66 GHz. A comparison was also made between the experimental measurements and theoretical calculations for silicon waveguide *B* for $d=1.8$ mm in Fig. 17(b). It is noted again that the experi-

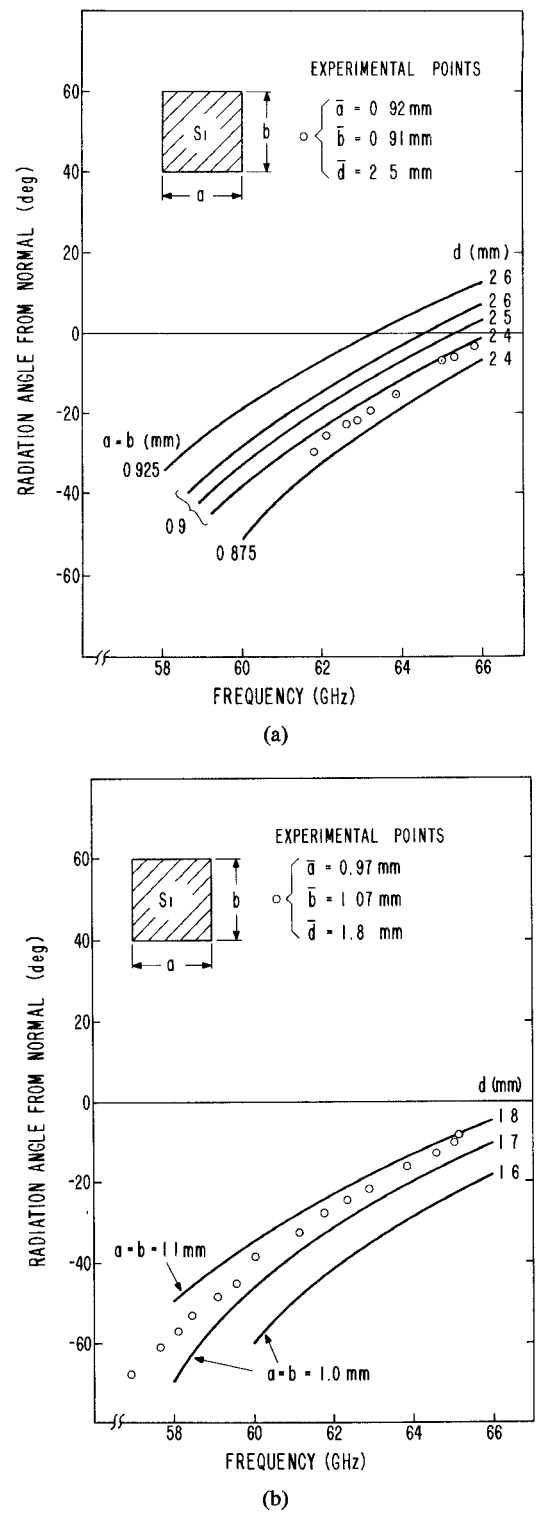

Fig. 17. Comparison of theory and experiment for radiation angle versus frequency for various guide sizes and perturbation spacings. (a) Silicon waveguide *A*. (b) Silicon waveguide *B*.

mental points occur at a more negative angle θ than the theoretical curve, indicating that experimental λ_g is, in both cases, greater than the theoretical λ_g. This agrees with previous direct measurements of λ_g using probe techniques [10].

V. Summary and Conclusions

Line scanning antennas were designed at millimeter-wave frequencies (55–100 GHz); the confirming experiments used rectangular silicon waveguides with metal stripe perturbations. Experiments indicated that a 3–9° beam of radiated power can be deliberately scanned through a range of angles by altering the input frequency. Using Marcatili's basic equations, the maximum and minimum waveguide sizes were determined allowing only the fundamental E_{11}^y mode for 60, 70, and 94 GHz. The key parameters of (1), guide wavelength λ_g and perturbation spacing d, were varied theoretically and experimentally to determine their effect and criticality to the angle of radiation and range of angular scan. The theoretical results show that the radiation angle is very sensitive to changes in λ_g, i.e., a 10-percent change causing an angular shift of approximately 15–20°. The guide wavelength in turn for a given material and frequency is determined by the physical dimensions of the guide with width a and height b.

Small changes in the spacing of the perturbations also can cause significant angular changes; 8° shifts occur for each 0.1-mm change in d. These results gave an indication as to how an antenna could be designed to cover a desired range of angular scan by altering the physical dimensions of the guide and/or changing the perturbations spacing.

Experiments were carried out to verify the calculated values of λ_g by detecting the standing wave pattern and measuring the distance between maxima, $\lambda_g/2$. In addition, λ_g was determined from (1) using experimentally measured angles of radiation. The experimental λ_g values are plotted in Fig. 16 and compared to the theoretical calculations. Both of the experimental techniques for determining λ_g indicate larger numerical values for any given frequency than theory would predict [10], [12]. Both techniques, however, show that the difference decreases as the frequency increases. The experimentally measured radiation angles for silicon waveguides A ($\bar{a}=0.91$ mm, $\bar{b}=0.92$ mm, $\bar{d}=2.5$ mm) and B ($\bar{a}=0.97$ mm, $\bar{b}=1.07$ mm, $\bar{d}=1.8$ mm) are plotted in Figs. 17(a) and 17(b), respectively. These angles are compared with theoretically calculated angles for guide sizes and perturbation spacings closely matching the average values.

The values for a, b, and d used in the theoretical calculations bracket the actual variation in parameters for the experimental waveguide antennas. The results show that the observed radiation angles fall within the theoretical limits and agreement is good, especially since the angle θ_n is very sensitive to changes in λ_g (and therefore a and b) and d.

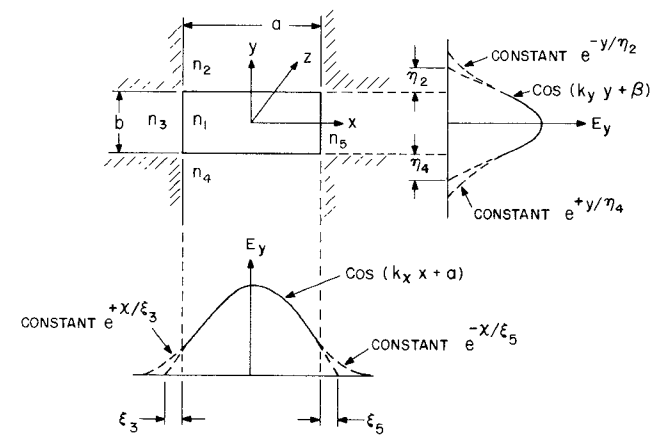

Fig. 18. Silicon waveguide n_1 immersed in different dielectrics n_2, n_3, n_4, n_5.

The feasibility has been shown of electronically scanning through a range of angles by varying the frequency fed into a relatively simple antenna structure consisting of a rectangular silicon rod with copper stripes (perturbations) attached to one surface, and how the range of scan can be altered by changing the physical dimensions of the guide and/or the spacing between perturbations.

Current investigations are underway on fixed frequency scanners, obtaining the change in radiation angle by modulating the effective dielectric constant of the silicon waveguide. This is being done by attaching a thin slab of silicon on the side surface of the antenna. The conductivity of this piece is modulated by dc injection in a p-i-n diode structure. As the conductivity is changed, λ_g changes, and, hence, the angle of radiation will be varied by electronic means.

VI. Appendix A
Calculation of Transverse Propagation Constants in Dielectric Waveguides

The mathematical equations which contain the transmission properties of a rectangular dielectric waveguide relate to the situation shown in Fig. 18. The index of refraction n_1 for medium 1 (silicon) is larger than that of the surrounding media (air) n_2, n_3, n_4, and n_5. If $n_2=n_3=n_4=n_5$, the field distributions will be symmetrical about the x and y plane as illustrated. Marcatili [6] developed the following basic equations.

$$k_1=\frac{2\pi}{\lambda_0}n_1=2\pi f\sqrt{\mu_1\epsilon_1} \tag{A-1}$$

and

$$k_z=\sqrt{k_1^2-k_x^2-k_y^2} \tag{A-2}$$

where k_1 = propagation constant in medium 1, k_z = axial propagation constant, k_x, k_y = transverse propagation constants in the x and y directions, $\mu_1=\mu_r\mu_0$ = permeability of medium 1 ($\mu_r=1$ for Si), and $\epsilon_1=\epsilon_r\epsilon_0$ = permittivity of medium 1 ($\epsilon_r=12$ for Si). The transverse propagation constants k_x and k_y are solutions of the transcendental

equations:

$$k_x a = p\pi - \tan^{-1}(k_x \xi_3) - \tan^{-1}(k_x \xi_5) \quad \text{(A-3)}$$

$$k_y b = q\pi - \tan^{-1}\left(\frac{n_2^2}{n_1^2} k_y \eta_2\right) - \tan^{-1}\left(\frac{n_4^2}{n_1^2} k_y \eta_4\right) \quad \text{(A-4)}$$

where a equals the x dimension (width) and b equals the y dimension (height) of the silicon waveguide and

$$\xi_{3,5} = \frac{1}{\sqrt{\left(\frac{\pi}{A_{3,5}}\right)^2 - k_x^2}} \quad \text{(A-5)}$$

and

$$\eta_{2,4} = \frac{1}{\sqrt{\left(\frac{\pi}{A_{2,4}}\right)^2 - k_y^2}} \quad \text{(A-6)}$$

where

$$A_{2,3,4,5} = \frac{\lambda_0}{2\sqrt{n_1^2 - n_{2,3,4,5}^2}}. \quad \text{(A-7)}$$

The number of extrema contained within the guide in the x and y directions are indicated by p and q, respectively. For the fundamental E_{11}^y mode, both p and q equal one. Fig. 18 illustrates that $\xi_{3,5}$ and $\eta_{2,4}$ are the distances the fields penetrate the respective surrounding mediums. $A_{2,3,4,5}$ indicates the maximum physical dimensions of the waveguide which will support only the fundamental mode provided the guide is surrounded by a uniform medium of equal refractive index. Equations (A-3) and (A-4) were solved exactly using a programmed calculator [7]. This was done by solving and plotting the right- and left-hand sides of each equation for a range of k_x and k_y values, respectively. The exact numerical values for k_x and k_y at the point of intersection (right-hand side of the equation equal to left-hand side) was determined by employing the "coarse grid approach" [13] to search for the minimum difference between the two curves for each equation.

A. Approximations

If the approximations of (4) are used, based on the fact that for well-guided modes most of the power will travel within medium 1 and the fact that the arctan and the argument of a small angle are approximately equal, (A-3) and (A-4) can be simplified to

$$k_x = \frac{p\pi}{a}\left(1 + \frac{A_3 + A_5}{\pi a}\right)^{-1} \quad \text{(A-8)}$$

and

$$k_y = \frac{q\pi}{b}\left(1 + \frac{n_2^2 A_2 + n_4^2 A_4}{\pi n_1^2 b}\right)^{-1}. \quad \text{(A-9)}$$

These equations can then be readily solved for k_x and k_y, and the guide wavelength calculated using (A-2) and

$$\lambda_g \equiv \lambda_z = 2\pi / k_z. \quad \text{(A-10)}$$

The agreement between λ_g (exact) and λ_g (approximate) improves as the wavelength becomes smaller with respect to the cross-sectional dimensions of the guide. This also means that more of the electric field stays within the waveguide boundaries.

ACKNOWLEDGMENT

The authors would like to thank F. King of the Ballistic Missile Defense Advanced Technology Center, Huntsville, Alabama, for his helpful discussions and encouragement.

REFERENCES

[1] A. A. Oliner, *Informal Communication*, Class Notes from Polytechnical Institute of New York.
[2] A. Hessel, "General characteristics of traveling-wave antennas," in *Antenna Theory: Part 2*, Collins & Zucker, Eds. New York: McGraw-Hill, 1969.
[3] M. M. Chrepta and H. Jacobs, "Millimeter-wave integrated circuits," *Microwave J.*, vol. 17, Nov. 1974.
[4] H. J. Kuno and Y. Chang, "Millimeter-wave integrated circuits," U.S. Army Electronics Command Final Report ECOM-73-0279-F, June 1974.
[5] Y. Chang and H. J. Kuno, "Millimeter-wave integrated circuits," U.S. Army Electronics Command Final Report ECOM-74-0454-F, Oct. 1975.
[6] E. A. J. Marcatili, "Dielectric rectangular waveguide and directional coupler for integrated optics," *Bell Syst. Tech. J.*, vol. 48, no. 7, Sept. 1969.
[7] K. L. Klohn, J. F. Armata, Jr., and M. M. Chrepta, "Transverse propagation constants in dielectric waveguides," *R & D Technical Report* ECOM-4242, U.S. Army Electronics Command, Fort Monmouth, NJ, Aug. 1974.
[8] J. E. Goell, "A circular-harmonic computer analysis of rectangular dielectric waveguides," *Bell Syst. Tech. J.*, vol. 48, no. 7, Sept. 1969.
[9] H. Jacobs, unpublished. (For methods used see [12].)
[10] H. Jacobs, G. Novick, C. M. LoCasio, and M. M. Chrepta, "Measurement of guide wavelength in rectangular dielectric waveguide," *IEEE Trans. Microwave Theory Tech.*, vol. MTT-24, pp. 815–820, Nov. 1976.
[11] T. Itoh, "Leaky-wave antenna and band reject filter for millimeter-wave integrated circuits," in *IEEE Int. Microwave Symp. Digest*, June 21–23, 1977, pp. 538–541.
[12] H. Jacobs, G. Novick, and C. M. LoCasio, "Probe measurements of guide wavelength in rectangular silicon dielectric waveguide," in *IEEE Int. Microwave Symp. Digest*, June 21–23, 1977, pp. 118–120.
[13] G. L. Neuhauser, *Introduction to Dynamic Programming*. New York: Wiley, 1967, pp. 104–111.